Dynamical diffraction of atomic matter waves by crystals of light

M. K. Oberthaler,[1,2] R. Abfalterer,[1] S. Bernet,[1] C. Keller,[1] J. Schmiedmayer,[1] and A. Zeilinger[1]
[1]*Institut für Experimentalphysik, Universität Innsbruck, Technikerstraße 25, A-6020 Innsbruck, Austria*
[2]*Clarendon Laboratory, University of Oxford, Parks Road, Oxford OX1 3PU, United Kingdom*
(Received 1 October 1998; revised manuscript received 29 January 1999)

Atoms in light crystals formed by a standing light wave are a model system to study the propagation of matter waves in periodic potentials. The encountered phenomena can be described by dynamical diffraction theory which has been extensively studied for x-ray, electron, and neutron scattering from solid state crystals. In this paper we show that an atomic de Broglie wave traversing a standing light wave allows investigation of predictions of dynamical diffraction theory which were previously experimentally not accessible. We present standard diffraction efficiency characterizations for *pure* absorptive and *pure* refractive crystals. Additionally we were able to measure *directly* the total atomic wave field formed inside a refractive and an absorptive crystal and to confirm the predicted *absolute* position of the atomic wave field with respect to the lattice planes. By superposing two standing light waves of different frequency we tailored a new kind of crystal potential where Friedel's law about usual diffraction symmetries is maximally violated. [S1050-2947(99)02207-6]

PACS number(s): 03.75.Be, 03.75.Dg, 42.25.−p

I. INTRODUCTION

Waves propagating inside a periodic medium are often encountered in physics. One of the anticipated phenomena is diffraction, which can be found, e.g., in x-ray scattering from solid state crystals [1]. A plethora of diffraction experiments have been performed which are in excellent agreement with the theory of dynamical diffraction.

The main difference between these diffraction experiments and our experiments is that in our situation the usual roles of matter and light waves are exchanged. We investigate propagation of atomic matter waves in a periodic light structure realized with a standing light wave. Closely related investigations have been described, for example, by Adams *et al.* [2], Balykin and Letokhov [3], and in Ref. [4]. Diffraction of matter waves at light fields makes the following new types of experiments feasible.

(1) With standing light waves one can produce perfect crystals of high purity consisting of *only* refractive or *only* absorptive structures without any crystal defects. Thus we are able to demonstrate very clearly the expected Borrmann effect [5], i.e., anomalously increased transmission at Bragg incidence through absorptive crystals [6].

(2) By setting up a thin on-resonant standing light wave one can realize an absorptive mask [7] which has the same periodicity as the crystal under investigation. Thus probing/masking techniques can be easily implemented in the experiment. With this technique we are able to retrieve the diffraction phase by measuring the total field of the atomic matter waves inside the crystal. Even the *absolute* position of the wave field and thus the absolute scattering phase can be deduced.

(3) A third new possibility is to tailor crystal structures which were not available previously [8]. This can be done by utilizing the fact that a pure refractive and a pure absorptive standing light wave can be superposed with arbitrary spatial phase. This represents the most general crystal structure for first order Bragg diffraction in the *weak* scattering limit.

Our experimental system consists of a well collimated atomic matter wave source, a mirror inside the vacuum system with precisely adjustable angular and spatial position, and an atom detector with good angular resolution. The standing light waves are realized by retroreflecting laser beams from the adjustable mirror. The theoretical framework is the theory of dynamical diffraction, which treats the wave inside the periodic structure as the coherent sum of all scattered wavelets. Originally, this theory was developed for the description of x rays propagating in perfect crystals [9]. Later it was adopted for electrons [10], and neutrons [11], traversing perfect crystals. Treating an extended standing light wave as a crystal in the sense of periodically arranged scatterers one can directly apply the known theoretical results to our system.

In the following section we will give a definition of a light crystal and discuss our diffraction regime. The third section is devoted to the dynamical diffraction theory applied to our situation of the propagation of atomic matter waves inside standing light waves. In Sec. IV we discuss how the atom-light system allows the realization of pure absorptive and pure refractive periodic structures. The experimental setup and measurement techniques are described in Sec. V. In the following sections the experimental results for scattered intensities and scattered phases are presented for pure refractive, pure absorptive, and combinations of refractive and absorptive crystals.

II. DEFINITION OF LIGHT CRYSTAL

In general, diffractive optical elements can be classified as thin or thick elements. The Talbot length [12], i.e., the characteristic scale of near field diffraction

$$L_{\mathrm{Talbot}}=\frac{2d^2}{\lambda}, \tag{1}$$

can be used as a characteristic length to distinguish between the two classes (λ represents the wavelength of the incoming wave, d is the periodicity of the diffracting element). The

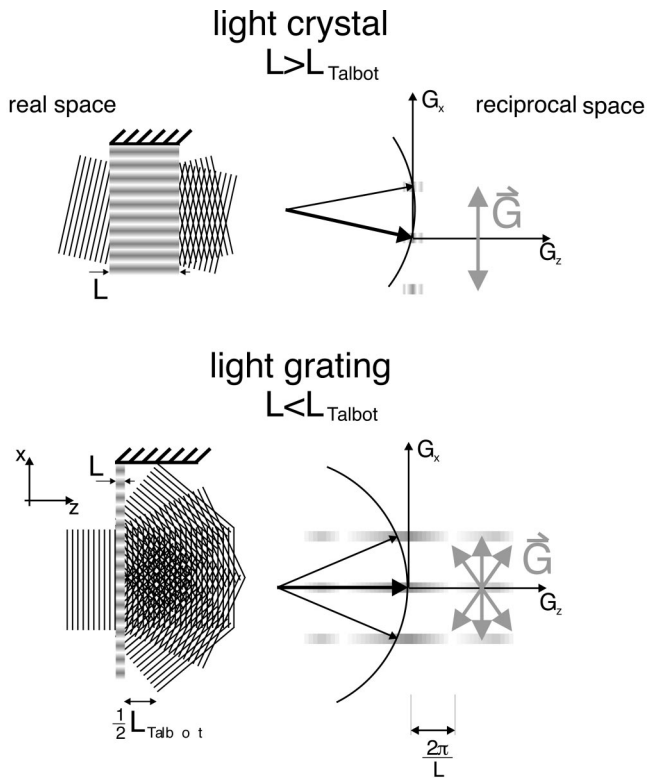

FIG. 1. The difference between thin and thick harmonic periodic structures in real and reciprocal space: In real space the Talbot length represents a boundary between both regimes. We would like to call a standing light wave with a transverse extent larger than the Talbot length a light crystal and for smaller extents a light grating. The different diffraction behaviors follow from the different lattice vector distributions depicted in the reciprocal space.

reason is that for gratings thicker than the Talbot length an atom, incident at the Bragg angle, traverses more than one grating plane. This situation cannot be described any more by a simple transmission function. Objects thinner than the Talbot length exhibit a weak dependence of their diffraction efficiency on the incident wave vector, i.e., on its direction and magnitude, whereas thick optical elements exhibit a very strong dependence on the incident wave vector.

This behavior can be understood for weak scattering with the description of diffraction in the reciprocal space introduced by Ewald [13]. It is based first on the energy conservation, implying that the incident and the diffracted wave vector have the same length, and secondly on momentum conservation, which requires that the incident wave vector can only change by multiples of the grating vector $\vec{G}$. The grating vector $\vec{G}$ corresponding to a given periodic structure of period d is found by the Fourier transform of the real space structure.

In a real crystal with a limited length L (z direction), the z component of the grating vector is uncertain in a range proportional to L^{-1}, whereas the x component (direction of the grating periodicity) shows a sharply defined, discrete spectrum spaced by $G=2\pi/d$. The diffracted intensities are given by the absolute square values of the corresponding Fourier transform amplitudes. In Fig. 1 the different situations encountered for a thin and a thick standing light wave are depicted in real and reciprocal space. Thus applying the Ewald construction [14] one finds that for thick elements only certain incidence angles can lead to significant diffraction amplitudes.

In analogy with optics we call a standing light wave with a longitudinal extent much smaller than the Talbot length a *light grating*. For standing light waves thicker than the Talbot length we would like to use the expression *light crystal* to emphasize the similarity to the diffractive behavior known for x rays, electrons, and neutrons in solid state crystals.

An additional distinction has to be made with respect to the potential height. As an approximate boundary one can use the characteristic grating recoil energy

$$E_g=\frac{\hbar^2\vec{G}^2}{2m}. \tag{2}$$

This is the kinetic energy a particle at rest with mass m gains when absorbing a grating momentum $\hbar\vec{G}$. Here we would like to make the distinction between the *Bragg regime* where the maximum potential energy of the light field is smaller than the grating recoil energy and the *channeling regime* for deeper potentials [15].

Classically this means that in the Bragg regime a particle impinging on the periodic structure under the Bragg angle will rattle over the potential maxima and the potential will act as a weak perturbation. In the channeling regime the particle will be confined between two lattice planes. This, however, happens only if the incidence angle of the particle is small enough, such that its momentum component in the direction of the grating vector is limited to a value where the particle is still reflected by the grating planes. Quantum mechanically this corresponds to bound states in the channeling regime, whereas the states in the Bragg regime (Bloch states [16]) are still unbound, but modified with respect to the continuum states of a free particle. This is the regime in which we are interested. There, Bragg scattering is observed and at most one diffracted wave is formed if the incidence angle matches the Bragg angle.

In the channeling regime the diffraction pattern exhibits a complicated dependence on the incidence direction and a wide angle distribution of the scattered atoms. This follows from the momentum distribution of the eigenstates which are the localized bound states.

III. DYNAMICAL DIFFRACTION THEORY

There are many different theoretical approaches to describe the propagation of a wave inside a periodic medium [14]. The main aim is to solve the underlying wave equation. In general the solutions are very complicated but for weak scattering the diffracted amplitudes can be described in good approximation analytically.

The main feature of extended weak periodic structures is that significant scattering is only observed if the incident wave impinges on the lattice planes at the Bragg angle θ_B,

$$\sin\theta_B=\frac{\lambda}{2d}, \tag{3}$$

where λ is the wavelength of the propagating wave and d is the spatial periodicity of the structure. This relation can be

derived by summing Huygens elementary spherical waves scattered by lattice planes. The calculation is easy if one ignores multiple scattering. This situation is described by the kinematic diffraction theory [14]. However, we are interested in the regime where multiple scattering occurs and each single scattering event leads only to a small scattered amplitude. This regime is described by the theory of dynamical diffraction.

There are many publications deriving the dynamical diffraction theory for all kinds of different waves directly from the wave equation. The first derivation was done by Ewald [9] in 1917 for x-ray waves propagating inside a solid state crystal. The derivation for electron matter waves inside a crystal was done by Bethe in 1928 [10] and for neutrons it was derived by Goldberger and Seitz in 1947 [11]. Consequently in this paper we would like to describe the theory only qualitatively and translate the rigorous results in the above mentioned papers for our experimental situation.

Dynamical diffraction theory describes the total wave field inside the periodic structure as a superposition of stationary wave fields. These so-called eigenfields can be described by a superposition of plane waves as was shown by Ewald [9]. The wave vectors are restricted by the periodicity of the scattering structure to the refracted incident wave vector (forward direction) and the refracted wave vector plus multiples of the grating vector (diffracted directions). An important feature of the eigenfields is that the relative amplitudes of the constituent plane waves depend on the angle between the forward scattering direction and the lattice planes. The evolution of the eigenfields is determined by the corresponding eigenenergy. Since different eigenfields have different overlap with the periodic structure (potential) the eigenenergies will differ. Thus within this approach the phenomenon of diffraction is described as an interference effect of different initially excited eigenfields. The scattered intensities are obtained as the result of interference of the corresponding amplitudes of the eigenfields.

The approach of eigenfields is very general and can be applied to any periodic potential. It is only in the *Bragg regime* that the propagation inside the potential is fully described by two eigenfields each consisting of two plane waves in the forward and Bragg scattering directions. Similar fields are used in the description of electrons in solid state physics and are called Bloch states [16]. In this framework the description is equivalent to a coupled two-state system. This is in contrast to the coherent channeling regime where the eigenfields consist of many plane waves and usually more than two eigenfields have to be used to describe the total wave field inside the periodic structure. In the following we will give the explicit form of the eigenfields in the two-beam approximation which is appropriate for weak scattering.

In order to make the results more compact we scale our experimental parameters. The potential is given in units of the grating recoil energy E_g. The incidence angle θ is described by the relative deviation θ^s from the Bragg angle $\theta_B = |G|/2|k| = \lambda_{dB}/2d$, where we use the small angle approximation for the Bragg angle ($\sim 20\ \mu$rad). The spatial thickness is given in units of the Talbot length $L_{\text{Talbot}} = 2d^2/\lambda$. The normalized parameters are

$$V^s = \frac{V}{E_g},$$

$$\theta^s = \frac{\theta_{\text{Bragg}} - \theta}{\theta_{\text{Bragg}}}, \tag{4}$$

$$z^s = \frac{z}{L_{\text{Talbot}}}.$$

The condition of weak potential implies $|V^s| < 1$, furthermore, our thick diffraction element criterion implies $z^s > 1$.

The eigenfields are (e.g., [17])

$$\psi_- = \psi_{\min} \propto [a_0^- + a_G^- e^{i\vec{G}\cdot\vec{r}}] e^{i\vec{K}_-\cdot\vec{r}},$$
$$\psi_+ = \psi_{\max} \propto [a_0^+ + a_G^+ e^{i\vec{G}\cdot\vec{r}}] e^{i\vec{K}_+\cdot\vec{r}}, \tag{5}$$

where $\vec{K}_\pm$ are the corresponding wave vectors inside the crystal. Note that the eigenfields are not normalized eigenstates, but are given in such a way that both fields are equally populated for an incident plane wave. Thus the whole diffraction behavior can be understood on the basis of these eigenfields. The relative amplitudes are given by

$$a_0^\pm = \frac{-\theta^s \pm \sqrt{\theta^{s2} + 4V_G^s V_{-G}^s}}{2V_G^s},$$
$$a_G^\pm = 1, \tag{6}$$

where $V_{\pm G}$ are the first Fourier components of the scattering potential defined via

$$V(\vec{r}) = \sum_{n=-\infty}^{\infty} V_{n\vec{G}} e^{in\vec{G}\cdot\vec{r}}. \tag{7}$$

The abbreviation $\psi_{\min}$ and $\psi_{\max}$ indicates that for exact Bragg incidence ($\theta^s = 0$) the two states have minimal and maximal overlap with the potential, respectively. It is important to note that the amplitude in the forward scattering direction depends on the potential height *and* on the deviation from Bragg incidence (see Fig. 2).

The difference of the wave vectors $\vec{K}_\pm$ for the two eigenstates follows from the different spatial overlap with the light intensity. This leads to a different potential energy of the atoms in the two states. The eigenenergies $E_\pm$ of the eigenfields are given by

$$E_\pm = E - V_0 + \frac{E_g}{2}\{\theta^s \pm \sqrt{\theta^{s2} + 4V_G^s V_{-G}^s}\}. \tag{8}$$

This relates the absolute magnitude of the wave vectors inside the medium $E_\pm \propto \vec{K}_\pm^2$ with the kinetic energy $E \propto \vec{k}^2$ of the impinging wave.

The direction of the waves inside the potential is restricted by the boundary conditions, since the wave function must be continuous over the boundary. This implies that the wave vector component parallel to the surface is the same inside and outside the crystal (indicated in Fig. 2). Classically speaking, momentum can only be transferred perpen-

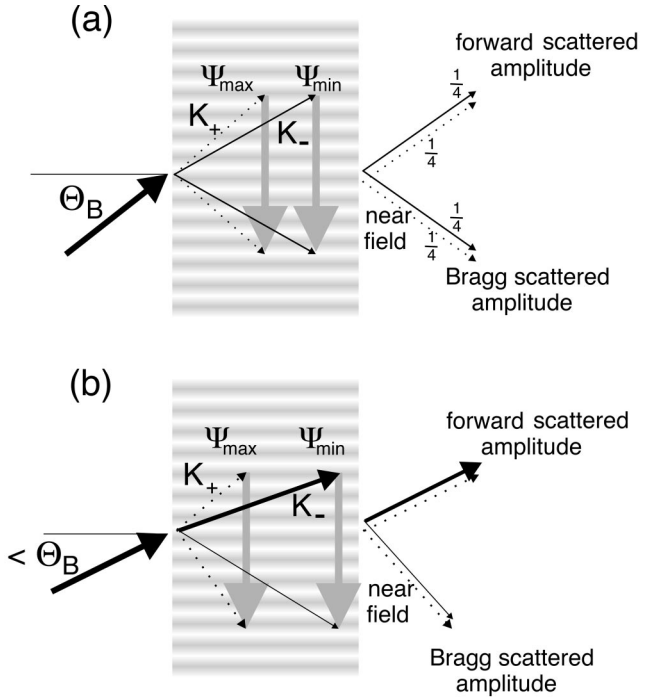

FIG. 2. The decomposition of a plane wave in eigenfields inside a periodic structure for (a) Bragg and (b) off-Bragg incidence. Dynamical diffraction theory leads to four plane waves propagating through the periodic structure. They can be merged to two eigenfields indicated by the same line style of the arrows. It is important to note that the eigenfields depend on the direction of the forward scattered field. In the graphs the amplitudes are symbolized with the width of the wave vectors.

dicular to a surface if there is no friction present. Choosing the coordinate system such that the surface is parallel to the x axis one finds

$$K_x = k_x,$$
$$K_z^{\pm} = \left[1 - \frac{V_0 + (E_g/2)(\theta^s \pm \sqrt{\theta^{s2} + 4V_G^s V_{-G}^s})}{2E}\right] k_z. \tag{9}$$

As the main result one finds that the periodic potential induces two different refractive indices for the two eigenfields. Thus the eigenfields propagate with different longitudinal velocities and hence accumulate a relative phase while traversing the periodic structure. The initial population of the eigenfields is determined by the boundary condition. In our experiments we analyze the propagation with a standard diffraction experimental setup where a collimated beam impinges with variable angle on a crystal surface. Thus for our experiment we have to decompose a plane wave incident at θ^s into the eigenfields. That leads to the amplitudes $A_\pm$ of the eigenfields $\psi_\pm$:

$$A_\pm = \frac{\pm V_G^s}{\sqrt{\theta^{s2} + 4V_G^s V_{-G}^s}}. \tag{10}$$

The total wave field inside the crystal is then given formally by

$$\psi_{\text{total}} = A_+ \psi_+ + A_- \psi_-. \tag{11}$$

All information about the diffraction behavior is contained in this total wave field. For example, the atom distribution at the end of a crystal of length L is given by the absolute square value of the total wave field $|\psi_{\text{total}}(L)|^2$. The intensity in the Bragg direction, I_G, and in the forward direction, I_0, is obtained by decomposing ψ_{total} into plane waves of the corresponding directions. It turns out that each diffraction direction gets contributions from both eigenfields (see Fig. 2). The observed scattered intensity is given by the interference of those amplitudes and depends for real potentials on the accumulated phase difference $\Delta\phi = (K_z^+ - K_z^-)L$ of the eigenfields during the propagation inside the crystal.

$$I_G = |A_+ e^{iK_z^+ L} + A_- e^{iK_z^- L}|^2,$$
$$I_0 = |A_+ a_0^+ e^{iK_z^+ L} + A_- a_0^- e^{iK_z^- L}|^2. \tag{12}$$

This is the basic description we will use to explain our experimental data. The result is applicable for real, imaginary, and complex potentials. Furthermore, it shows that in the weak coupling limit of first order Bragg diffraction only the first Fourier components of the potential are essential for the description of the propagation. Thus we would like to emphasize that the experimentally used *sinusoidal* complex potential which has only zero and first order Fourier components exhibits all features expected for an arbitrary complex periodic potential in this limit.

IV. LIGHT CRYSTAL CHARACTERISTICS

In this section we discuss what kind of potentials can be realized with near resonant light for a specific internal atomic state.

For an open two-level system as shown in Fig. 3 the interaction of the atom in state $|1\rangle$ with the near resonant classical electromagnetic field $E(\vec{r},t)$ can be described by the action of the optical potential given by Chudesnikov and Yakovlev [18],

$$V(\vec{r}) = \hbar \frac{\Omega_{\text{Rabi}}^2(\vec{r})}{4\Delta + i2\gamma_{e2}}, \tag{13}$$

where $\Omega_{\text{Rabi}}(\vec{r})$ represents the on-resonance Rabi frequency, which is periodically modulated in space for a standing light wave. The detuning of the laser frequency from resonance is described by $\Delta = \omega_l - \omega_0$, where ω_l is the laser frequency and ω_0 is atomic transition frequency. The parameter γ_{e2} is the decay rate from the excited state $|e\rangle$ to the ground state $|2\rangle$. The imaginary part of this potential describes the loss of the population from the initial state $|1\rangle$ to the experimentally distinguishable ground state $|2\rangle$ via optical pumping. This loss can be regarded as an absorption mechanism for atoms in the internal state $|1\rangle$. The spectral shapes of the imaginary and real parts of the complex potential are indicated in Fig. 4.

One has to keep in mind that this form of the potential can only be applied if two basic assumptions are fulfilled. First the spontaneous decay of the excited state back to the initial state $|1\rangle$ described by γ_{e1} has to be negligible compared to γ_{e2}. Secondly the population of the excited state has to fol-

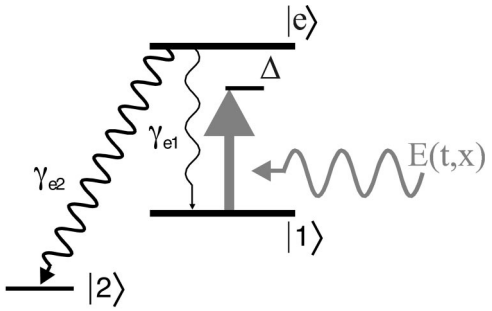

FIG. 3. The basic level scheme to realize a complex optical potential for an atom in state $|1\rangle$ interacting with a near resonant light field: The optical pumping process to state $|2\rangle$ leads to a loss of population in state $|1\rangle$. This pumping process can be regarded as an absorption process for an atom in state $|1\rangle$.

low the ground state population instantaneously. This is usually called the secular approximation and leads to good results for situations with $\Omega_{\mathrm{Rabi}}<|\Delta+i\gamma/2|$.

For our experiments we use metastable argon with the level scheme as given in Fig. 5. This offers a closed transition from the $1s_5$ to the $2p_9$ state at 811 nm and an open transition from the $1s_5$ to the $2p_8$ state at 801 nm. There the excited state decays with 72% probability to the nondetected and hence distinguishable ground state. The rate of 28% back to the metastable state leads to a reduced absorption for a given laser intensity as expected from Eq. (13). By integrating the Bloch equations a reduction factor of 0.55 was found.

To illustrate the effect of an absorptive potential we performed an experiment measuring the transmission of atoms through a 3 cm thick light wave tuned exactly on resonance for far off-Bragg incidence. The observed absorption as a function of light intensity is shown in Fig. 6. Clearly an

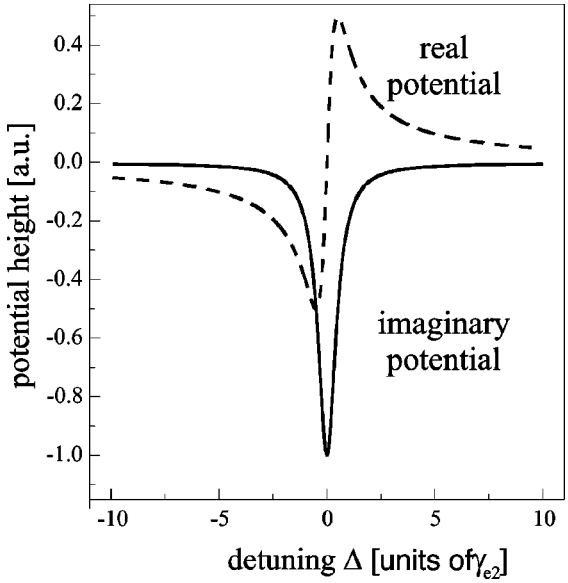

FIG. 4. The light potential as a function of the frequency difference Δ of the light field and the atomic transition. The action of the potential on the atom can be described via a refractive index proportional to the potential. For exact resonance, only an imaginary potential is present while for large detunings the real part of the potential dominates.

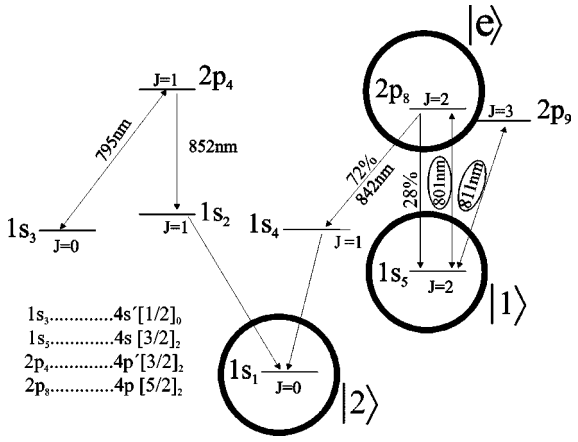

FIG. 5. The level scheme of metastable argon: The three-level system used is indicated with the circles. The levels are labeled by the Paschen notation and the total angular momentum *j*. The table relates the Paschen notation used throughout the paper to the standard spectroscopic notation.

exponential behavior is seen over three orders of magnitude, as is expected from Beer's law. This can be deduced using the results of Sec. III in the limit of $\theta^s\rightarrow\pm\infty$. One finds

$$I_{\mathrm{trans}}=\left|e^{-i(V_0/2E)k_z z}\right|^2=e^{-\kappa z}, \tag{14}$$

where V_0 is the purely imaginary dc Fourier amplitude of the potential (average strength), E the total incidence kinetic energy, and $\kappa=|V_0|k_z/E$ is the average absorption coefficient usually used in Beer's law. The solid line represents the expected behavior given by Eq. (14) modified by the reduction factor found by solving the Bloch equation. The deviation for very weak light intensities results from the fact that the Rabi cycles become longer than the interaction time. In this case a quadratic behavior as a function of intensity is ex-

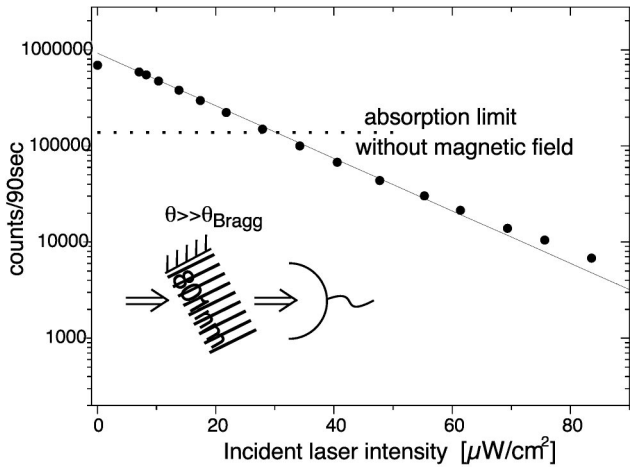

FIG. 6. Experimental result for the total transmission of atoms through a constant light field resonant with the open transition at 801 nm, as a function of the laser intensity: The transmission decreases exponentially according to Beer's absorption law. The dotted line shows the absorption limit without any magnetic field due to the dipole selection rule for the $J=2\rightarrow J=2$ transition used. In our experiment the Earth's magnetic field and the long interaction time lead to an equal interaction of all magnetic sublevels with linearly polarized light.

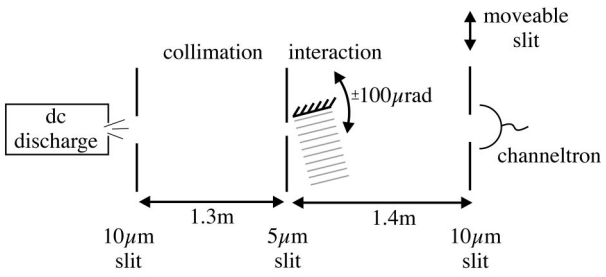

FIG. 7. Scheme of the experimental setup: A gas discharge is used to produce metastable argon atoms. Collimation with two slits leads to an atomic beam with a transverse coherence length of about 2 μm. The standing light wave is realized by retroreflecting an expanded laser beam from a mirror situated inside the vacuum chamber. The atoms are detected with a channeltron and the spatial resolution of the far field was obtained by a moving slit in front of the detector.

pected. In the experiment we used linearly polarized light resonant with the $1s_5 \rightarrow 2p_8$ transition. Since our atomic beam is unpolarized (statistical mixture of magnetic sublevels) the dipole selection rules for a $J=2 \rightarrow J=2$ transition imply that 1/5 of the atoms ($m_j=0$) do not interact with the light at all. This limit is indicated with the dotted line in Fig. 6. Clearly we observe that all magnetic sublevels interact on average in the same manner with the linear polarized light field which can be explained by the continuous mixing of the magnetic sublevels due to the Earth's magnetic field. Hence we can neglect the internal magnetic sublevel structure for the description of the metastable argon atom and describe it as an effective open two-level system.

V. EXPERIMENTAL SETUP AND MEASUREMENT TECHNIQUES

Our experimental setup, schematically shown in Fig. 7, is a standard atomic beam apparatus adapted to resolve the tiny diffraction angles (≈ 20 μrad) expected for the argon atoms passing through a standing light wave. Furthermore, the incidence angle of the atoms at the standing light wave is adjustable with μrad resolution by changing the angle of the retroreflecting mirror.

As a matter wave source we use a thermal metastable argon beam. The metastable argon atoms are prepared in a dc gas discharge [19]. Their average wavelength is in the range of $\lambda \sim 12$–17 pm (corresponding to a velocity of 500–700 m/sec) depending on the source parameters. The source produces atoms in the $1s_3$ and $1s_5$ metastable states with a ratio of $\sim$15/85. Only these metastable atoms can be detected by our channeltron detector. The background due to the atoms in the $1s_3$ state is eliminated by optically deexciting those atoms with a laser diode at 795 nm. The lifetime of the remaining $1s_5$ metastable atoms is on the order of 40 s and thus much longer than the atomic time of flight (≈ 4 ms) through the beam line. The atomic beam is collimated with a set of two slits (10 μm, 5 μm) at a distance of 1.3 m. This leads to a residual divergence of the atomic beam of ± 8 μrad.

The light crystals are realized by retroreflecting an expanded Gaussian laser beam with a full width at half maximum (FWHM) intensity distribution of 3.5 cm from a gold mirror. The far off-resonant standing light waves were realized with a titanium sapphire laser. A laser diode was used for on-resonant experiments. The mirror surface defines the lattice planes because the metallic mirror surface defines a node of the standing light wave. Thus, by rotating the mirror, the incidence angle with respect to the lattice planes could be changed. Small angular tilts in the range of ± 100 μrad $\approx 5\theta_B$ were accomplished by a piezo actuator built into a commercial mirror holder.

The far field diffraction pattern and thus the angular distribution of the scattered intensity was measured 1.4 m downstream by moving a 10 μm slit in front of the channeltron, which registered only metastable atoms. Therefore, the state selective measurement necessary for the realization of a complex potential (see Sec. IV) was intrinsically given by our detection scheme.

As a standard characterization of the diffraction phenomena in crystal physics, rocking curves are measured. These represent the scattered intensities as a function of the incidence angle of the beam. In our experiment this was accomplished by fixing the detection slit at a certain position in the far field observation plane. The incidence direction was changed by tilting the mirror with respect to the atomic beam.

We used two additional measurement techniques to extract information about the phase between the forward and the Bragg scattered amplitudes shown in Fig. 8. One is a compact two-crystal-interferometer setup where the two outgoing beams are superposed with an adjustable relative phase. The other utilizes a mask with the same period as the potential. By moving the mask right over the exit surface of the crystal and measuring the total transmission one can probe the atomic wave field.

Experimentally we realized these phase measurements with two standing light waves at two different wavelengths retroreflected from the same mirror surface. The gold mirror surface defines nodes for both standing light fields, thus both light crystals are in phase at the mirror surface. However, the relative phase changes as a function of distance from the mirror due to the different spatial period of the two crystals as indicated in Fig. 8. We used two transitions from the metastable $1s_5$ state of argon, namely, 801 nm ($A_{ik}=9.6\times10^6$ s^{-1}), and 811 nm ($A_{ik}=36.6\times10^6$ s^{-1}). This leads to a spatial beating of the relative phase with a period of 32.34 μm. This distance is much larger than the atomic beam diameter (5 μm). Thus, by changing the distance of the mirror surface to the atomic beam one can vary the relative phase between the two periodic structures at the incidence position of the atomic beam. A mirror shift of 32.34 μm corresponds to a relative phase change of 2π equivalent to a relative spatial displacement of one grating period between the two standing light waves. This method is analogous to the Vernier principle used for length measurements. There, a combination of two rulers with slightly different periods leads to a fine spatial resolution.

The interferometric setup was realized by two successive thick (~ 2 cm) standing light waves, where the first crystal was set up with 801 nm light and the second with 811 nm. The detection slit was positioned such that only first order diffracted atoms were registered. Their intensity was ob-

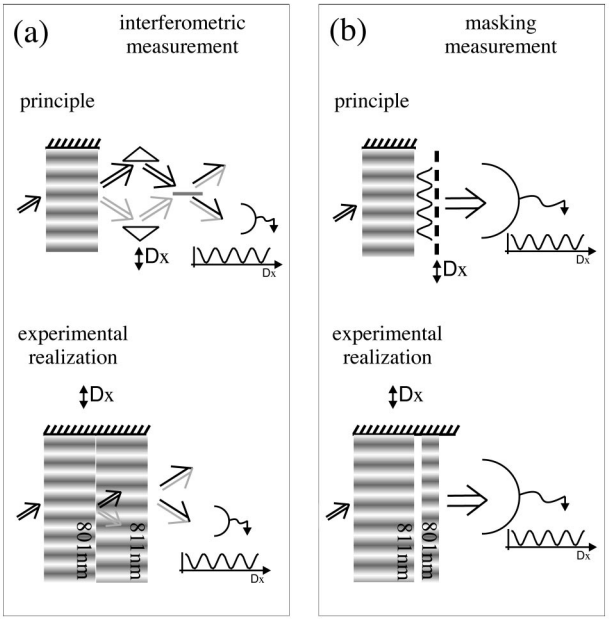

FIG. 8. Measurement techniques used to retrieve phase information about the scattered amplitudes: A two-crystal interferometer (a) directly recombines the forward and Bragg scattered beams. An observation of a fringe pattern of the combined Bragg scattered intensity demonstrates the coherence of the scattering process. Changes in the scattering phase are detected as a shift of the interference fringes. The masking technique (b) yields information about the atomic density distribution after the first object. Experimentally the two periodic structures are realized by retroreflecting light of different wavelength from the same mirror. Thus the relative phase between the two objects changes as a function of distance to the mirror surface.

served as a function of the mirror position, measured with a position encoder (Heidenhain, with an accuracy of ± 0.5 μm), and varied with a translation stage driven by a dc motor (Oriel).

For the other technique, i.e., the masking, the first crystal (~ 3 cm) was realized with a light frequency at 811 nm far off resonance (with a typical light intensity of 40 mW/cm^2 at a detuning of 5 GHz from resonance). The probing mask was created directly behind the phase crystal by focusing resonant (absorptive) 801 nm laser light at the surface of the mirror (~ 1 mm wide). There, the typical light intensity was 40 μW/cm^2, resulting in an average transmission of $\approx 10\%$ through the grating. Then the integral transmission through the two successive gratings was measured. By shifting the mirror into the atomic beam path the shadow of the mirror could be detected, in order to determine the absolute position of the mirror surface, which defines a common node for both light structures. This means that one can experimentally determine a position where the two periodic structures are in phase. Since the beam profile is 5 μm wide this position can be measured with an accuracy of ≈ 2 μm which is 1/15 of the periodicity. This allows measurements of the absolute position relative to the lattice planes with a resolution of 24 nm. The same principle was also used to create *complex* light crystals by collinearly superposing light from two different lasers (tuned at the two different atomic transitions at 801 nm and 811 nm, respectively), at a beam splitter cube in front of the beam expander. This produced two *overlapping* standing light fields with a spatially varying phase difference, due to the beating of the different grating periods. By translating the common retroreflection mirror, any spatial phase relation between the two superposed light crystals could be adjusted, providing the possibility for generating complex potential modulations, as will be explained later.

VI. REFRACTIVE CRYSTAL

In this section we present the experimental results concerning scattering off a pure refractive extended periodic structure, and we will compare them to dynamical diffraction predictions.

From the light potential introduced in Sec. IV it becomes clear that a standing light wave with a detuning from resonance much larger than the natural linewidth can be regarded as a pure real periodic potential. Thus a far detuned thick standing light wave can be described as a pure refractive crystal. This case has already been investigated in some detail by other groups [20].

For the description within the framework of dynamical diffraction theory the Fourier amplitudes of the periodic structure are of relevance. For the pure sinusoidal phase crystal they are given by

$$V_0 = \frac{V_{\max}}{2},$$

$$V_G = \frac{V_{\max}}{4} e^{i\alpha}, \tag{15}$$

$$V_{-G} = \frac{V_{\max}}{4} e^{-i\alpha},$$

where $V_{\max}$ represents the potential maximum. The phase α determines the spatial position of the crystal. The dc Fourier component V_0 is real, and the first Fourier components are complex conjugates of each other.

A. Scattered intensity measurements

The experimental results for the scattered intensities are shown in Fig. 9. The left graph shows the scattered intensity in the far field for different incidence angles. The data demonstrate that only for special incidence angles, namely, the Bragg angles θ_B, is significant Bragg scattered intensity observed. The position of the peak corresponding to Bragg scattered atoms depends on the incidence angle. This is due to the velocity distribution of the incident beam. Fast atoms are Bragg scattered at smaller incidence angles, and are detected closer to the forward scattered intensity than slow atoms.

Rocking curves represent the scattered intensity as a function of the incidence angle. First of all, the integral transmitted intensity exhibits no dependence on the incidence angle as expected from particle conservation (upper right graph in Fig. 9). The Bragg feature is revealed by measuring the scattered intensities individually in the forward and Bragg directions.

The rocking curve for the forward scattered intensity is measured by positioning the detection slit (10 μm) at the

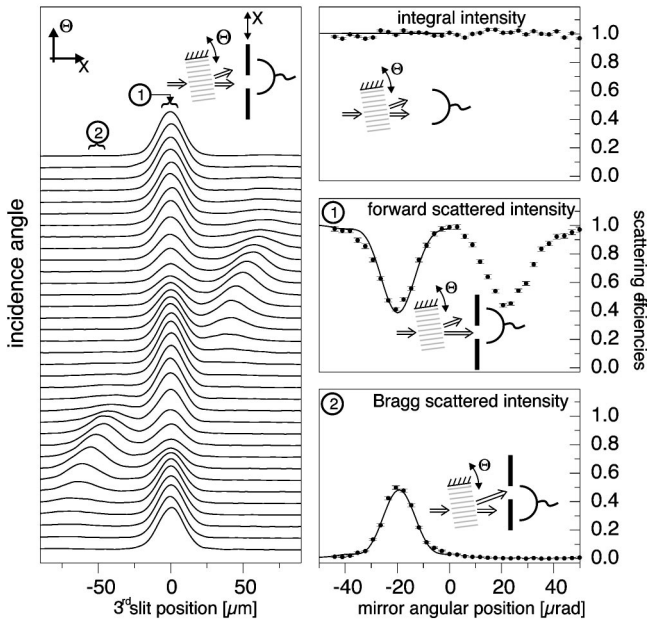

FIG. 9. Experimental investigation of Bragg diffraction at a refractive crystal: The left graph shows the measured far field (diffraction pattern) for different incidence angles. The scattered intensities as a function of the incidence angle are shown on the right side of the figure. The solid lines are the predictions of dynamical diffraction theory.

position of the forward (undiffracted) beam. The observed intensity exhibits two minima as can be seen in Fig. 9. They result from the loss of atoms due to diffraction at the two conjugated first order Bragg angles. If the detection slit is located at the Bragg angle one observes a diffraction peak only for the corresponding Bragg incidence. Note that the sum of the forward and the Bragg scattered intensities in such a measurement is not unity, since different velocities have different diffraction angles. Thus only a certain velocity class will pass through the third slit situated at the maximum of the Bragg peak.

The solid lines in Fig. 9 are the results of dynamical diffraction theory. In order to get this excellent agreement one has to take into account the diffraction pattern change in the observation plane due to the velocity distribution, furthermore, the dependence of diffraction efficiency on the incident wavelength and also the angular distribution of the incident beam. The only fit parameter for this experiment was the potential height, where $V_{\max}=0.6E_g$ leads to the theoretical results shown in Fig. 9.

B. Diffraction efficiency: The Pendellösung phenomenon

The Pendellösung phenomenon describes an exchange of the intensities in the forward and Bragg scattered beams usually as a function of crystal length. The term Pendellösung phenomenon points out that this effect is analogous to the energy exchange between two coupled pendulums. This effect is usually analyzed in the eigenmode basis of the system. In a similar manner dynamical diffraction describes the propagation of a wave inside the periodic medium.

The scattered intensities are obtained as a coherent superposition of two amplitudes with a certain relative phase. Using Eq. (12) in Sec. III one finds for the Bragg scattered intensity I_G and the forward scattered intensity I_0

$$I_G(z,V_G,\theta)=\frac{\sin^2\left[2\pi|V_G^s|z^s\sqrt{\frac{1}{4}(\theta_i^s/|V_G^s|)^2+1}\right]}{\frac{1}{4}(\theta_i^s/|V_G^s|)^2+1},$$
$$I_0(z,V_G,\theta)=1-I_G(z,V_G,\theta). \tag{16}$$

The scattered intensities exhibit a rich dependence on various experimentally adjustable parameters. In Fig. 10 a comprehensive illustration of the dependencies is given. The main graph shows the Bragg scattered intensity as a function of the incidence angle for the scaled parameters $z^s=2$ and $V_G^s=0.125$. The parameters are chosen such that for Bragg incidence all atoms are diffracted. Equal markers in Fig. 10 represent equal parameter sets in the different graphs. The angular dependence exhibits a damped Pendellösung-like behavior. The inset graphs show the dependence of the diffraction efficiency on the crystal length and on the potential height for on- and off-Bragg incidence. The mechanism of the population exchange between the two forward and Bragg scattered states is analogous to the well known Rabi oscillations of the population between ground and excited states of a two-level atom interacting with light. Theoretical investigations of this effect can be found, for example, in Bernhardt and Shore [21].

Experimentally the Pendellösung phenomenon was demonstrated as a function of crystal length by Sippel *et al.* [22] for Bragg scattering of neutrons at perfect crystals. Equivalently one can observe the Pendellösung phenomenon by changing the wavelength of the incident wave, because the scaled length z^s is proportional to λ. This was demonstrated by Shull [23] for neutrons in perfect crystals.

In atom optics the Pendellösung phenomenon is usually demonstrated as a function of potential height [20]. In this section we would like to apply dynamical diffraction theory to this problem and compare the predictions with our experimental results.

We have qualitatively observed the expected structure within a rocking curve. The experimental data are shown in Fig. 11. There we measure the forward scattered intensities for different potential heights. We detect the forward scattered beam, since no additional structure can be observed in the diffracted beam due to the velocity distribution of the atoms. As can be seen in Fig. 11 the absolute diffraction efficiencies are reasonably well explained by dynamical diffraction theory as discussed in Sec. III. All six graphs are simultaneously fitted with one free parameter, namely, the detuning of the laser frequency. The deviation between the experimental results and the theory is due to the breakdown of the two-beam approximation for high potentials.

For exact Bragg incidence the Bragg scattered intensity varies in the same way by changing the crystal thickness z or the potential modulation height V_G. The Pendellösung behavior as a function of crystal thickness is exclusively due to the increasing accumulated phase difference of the two populated eigenstates. Their energy difference increases for off-Bragg incidence. This implies that for a given crystal thickness the accumulated phase difference is larger for off-Bragg incidence than for Bragg incidence. This explains the shorter

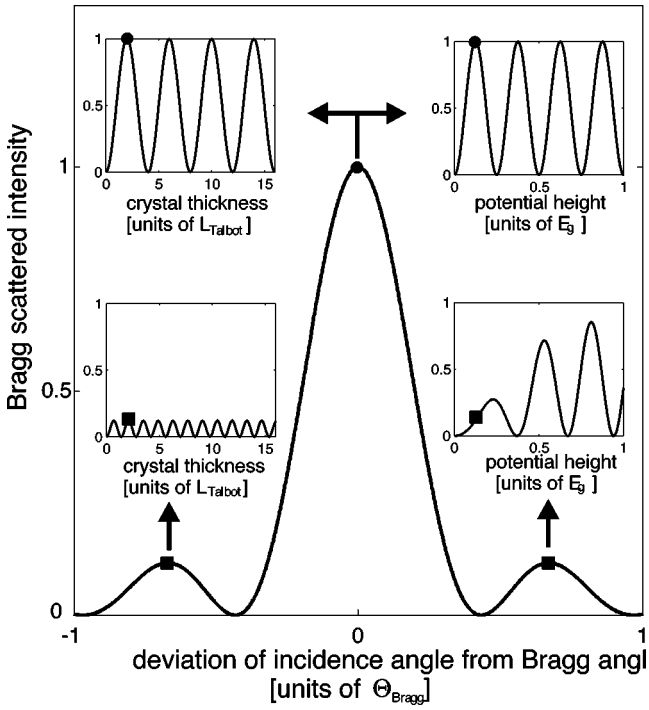

FIG. 10. Summary of the dependencies of the Bragg scattered intensity for a phase crystal [according to Eq. (16)]: The main plot shows the angular dependence for crystal parameters of $z^s=2$ and $V_g^s=0.125$ leading to a 100% diffraction efficiency for exact Bragg incidence. As indicated in the upper insets the scattered intensity exhibits a sinusoidal behavior as a function of crystal thickness and potential height. For off-Bragg incidence the behavior is different due to the fact that the eigenfields depend on the potential height while they are independent of the crystal thickness. Equal markers in the different graphs correspond to equal experimental situations.

Pendellösung length for increasing deviation from the Bragg angle (see lower left inset in Fig. 10). The smaller Pendellösung amplitude is due to the decrease of the Bragg scattered amplitude in the total wave field (see Fig. 2).

The Pendellösung phenomenon as a function of potential height is slightly more complicated. By changing the potential height both the eigenenergies and the eigenfields change. Only for the special case of exact Bragg incidence does the dependence on potential height enter exclusively via the accumulated phase difference. For off-Bragg incidence one has to consider the eigenenergies as well as the eigenfields. It turns out that the angular dependence of the eigenfields becomes less pronounced for higher potentials. Thus for a sufficiently high potential the off-Bragg Pendel effect is again mainly given by the accumulated phase difference. This explains why the Pendellösung phenomenon exhibits for higher potentials the full modulation even for off-Bragg incidence as revealed in the lower right inset in Fig. 10. Our experimental results shown in Fig. 12 demonstrate the expected behavior for the Pendellösung phenomenon as a function of potential height for different incidence angles. We used a far off-resonant 811 nm standing light wave as a phase crystal. In order to reduce the velocity distribution the measurement was carried out with a time of flight selection by pulsing the discharge and setting a gating window such that only atoms within the velocity range of 650–850 m/sec were detected. Consequently a high diffraction efficiency of up to 80%

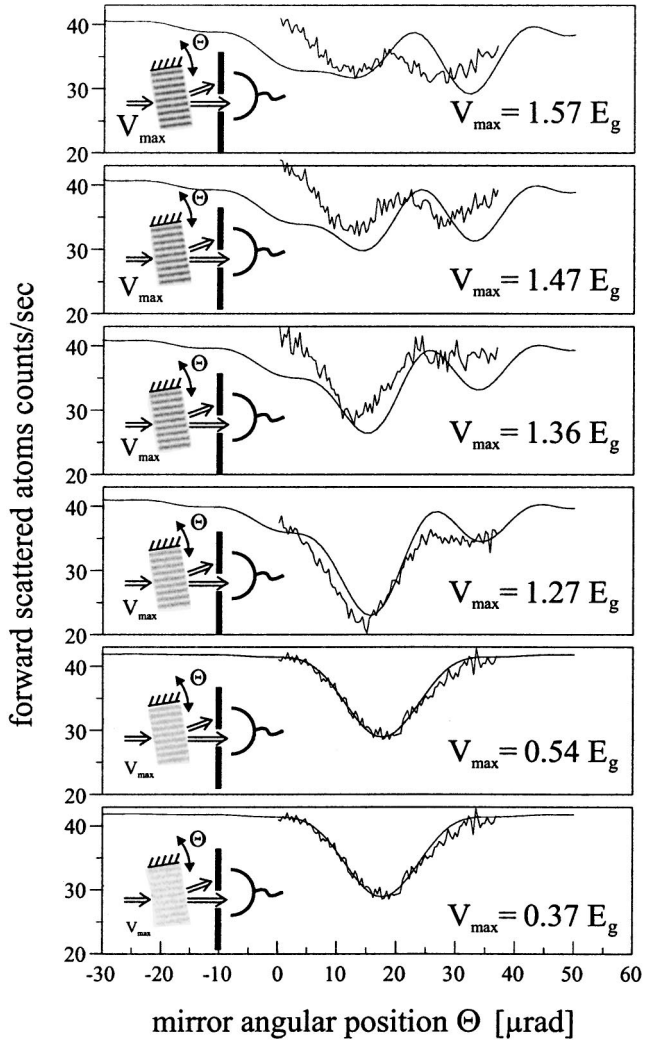

FIG. 11. Experimental results for the rocking curve of the forward scattered intensity for different potential heights: As expected from dynamical diffraction theory a structure within the Bragg acceptance angle is observed. The solid lines represent the results of dynamical diffraction theory within the two-beam approximation taking into account the velocity and angular distribution of our atomic beam. The deviation for higher potentials might be understood within a multiple-beam treatment.

could be experimentally observed in contrast to 60% diffraction efficiency without velocity selection.

In Fig. 12 the x axis is directly proportional to the measured laser intensity, scaled by an intensity of 38 mW/cm^2 which yields a light potential corresponding to a grating recoil energy at our frequency detuning of 5 GHz (saturation intensity: 5.8 mW/cm^2). Taking into account the Gaussian profile and the reflection at the entrance window one ends up with 28 mW/cm^2 light intensity uniformly distributed over the beam profile. Thus, the data agree with our model within our experimental accuracy of frequency determination (using a Burleigh wave meter). Deviations from the expected behavior at both larger incidence angles and higher light potentials indicate that the employed two-beam approximation breaks down in these regimes. Furthermore, a damping of the Pendellösung oscillations occurs due to the limited longitudinal and transverse coherence of the atomic beam, i.e., its velocity distribution and its angular divergence, respectively.

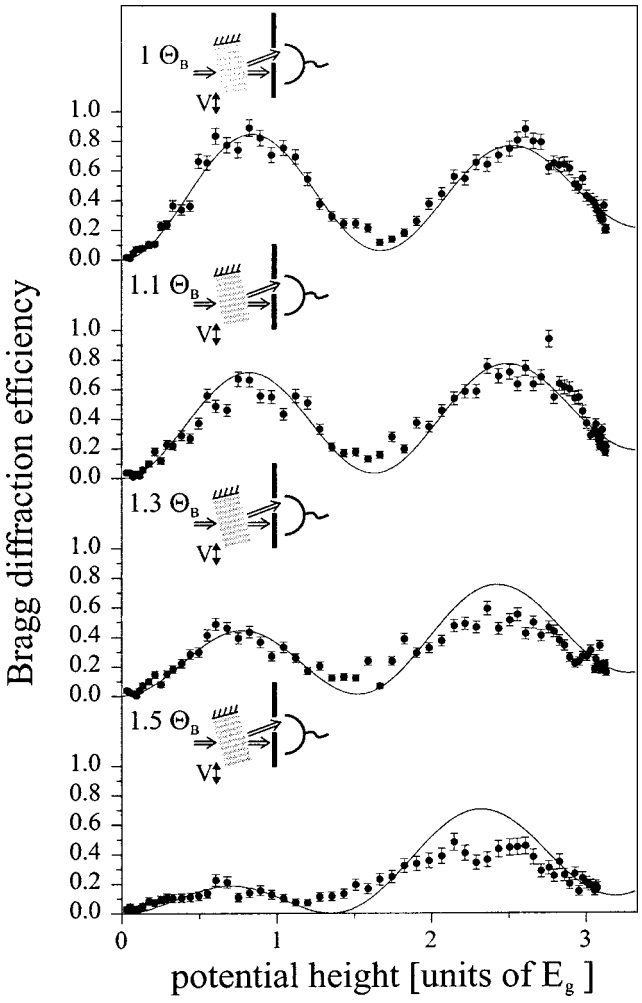

FIG. 12. Experimental demonstration of the Pendellösung phenomenon as a function of potential height for different incidence angles: The solid lines represent the predictions of dynamical diffraction theory.

C. Scattering phase measurement

In standard diffraction experiments usually only intensities are measured. By using the interferometric setup described in Sec. V we were also able to measure the phase difference between the forward and Bragg scattered beams.

The experimentally observed interference patterns with the two-crystal interferometer are shown in Fig. 13. Both standing light waves were detuned from resonance and thus can be described by two phase crystals. The relative *spatial* phase $\Delta\Phi$ between the crystals was adjusted by changing the distance of the mirror surface to the atomic beam. The first crystal was thinner (thicker) than half of the Pendellösung length $\Lambda = L_{\mathrm{Talbot}}/V_G^s$ for the upper (lower) trace shown in Fig. 13, whereas the potential of the second crystal was held constant in the two experiments. The interference fringes clearly confirm the coherence of the scattering process in the phase crystals. Increasing the length of the first crystal over half of the Pendellösung length by changing the laser intensity results in a π phase jump of the observed interference fringes.

The two experimentally observed fringes in Fig. 13 can be directly understood on the basis of the total wave field which is formed inside the crystal. For Bragg incidence the total

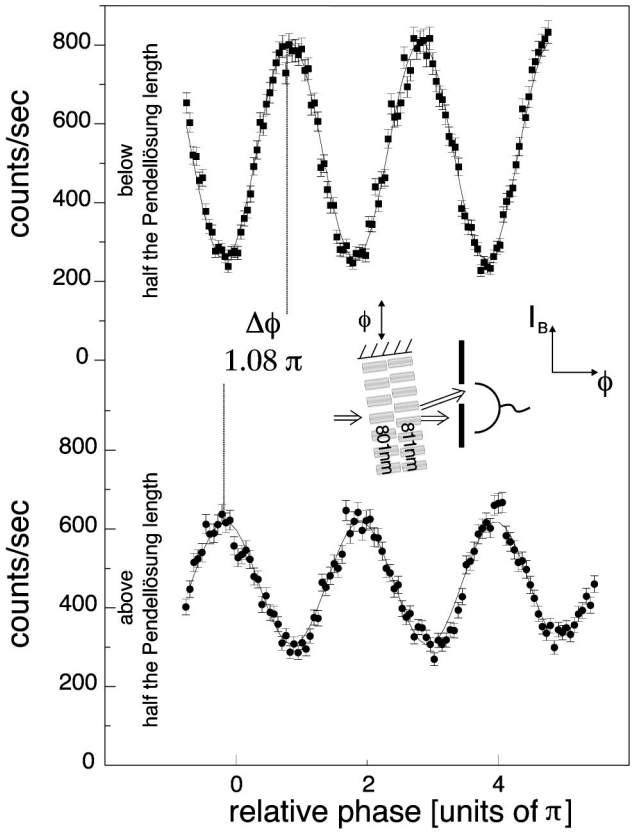

FIG. 13. Experimental results of the two-crystal interferometer consisting of two successive phase crystals. The solid curves are a fit to the data. The upper trace shows the Bragg diffracted intensity as a function of the relative *spatial* phase Φ between the two crystals. Increasing the laser intensity of the first standing light wave ($>1/2$ Pendellösung intensity) one observes the interference fringe plotted below. The observed phase jump of $\Delta\Phi \approx \pi$ is predicted by dynamical diffraction theory.

wave field inside a refractive crystal is given by

$$\psi_{\mathrm{total}} = \frac{1}{2}\psi_{\max} - \frac{1}{2}\psi_{\min} = \cos\frac{G}{2}x - e^{-i\Delta\phi} i \sin\frac{G}{2}x, \quad (17)$$

where $\Delta\phi = (K_z^+ - K_z^-)L$ is the phase difference between the two eigenfields accumulated during their propagation through the crystal of length L. This leads to an atomic density distribution inside the crystal of

$$|\psi_{\mathrm{total}}|^2 = 1 + \sin\Delta\phi \cos\left(Gx + \frac{\pi}{2}\right) \quad (18)$$

for a potential of the form

$$V = \frac{V_{\max}}{2}(1 + \cos Gx). \quad (19)$$

It should be mentioned that the normalization of the wave functions is arbitrary, since for the calculation of all measurable quantities only relative changes in the wave amplitudes are essential. Comparing the potential in Eq. (19) and the total wave field in Eq. (18) shows that the atoms leave the light crystal mainly at the steepest positive or negative gradient of the potential. The sign of the gradient at which the atoms emerge depends on the sign of the phase factor in Eq.

(18), i.e., the absolute outlet position of the atoms for crystal thicknesses smaller than the Pendellösung length is at the flank on which the incident plane wave impinges. Changing the potential such that the thickness of the crystal is larger than half of the Pendellösung length implies that the accumulated phase difference $\Delta\phi$ is larger than π. In this case the sine term in Eq. (18) changes sign, which implies that the wave field jumps by half of the grating period. Since this is a phase flip the visibility of the wave field has to be zero at a phase difference $\Delta\phi=\pi$. This is indeed the case, since for this phase difference the only emerging beam consists of Bragg scattered atoms, and thus the wave field is just a plane wave.

In the following we want to present our results which confirm the expected *absolute* position of the wave field. For this purpose we use the masking technique (see Sec. V) with a thin absorptive light grating. As a refractive crystal we used a far off-resonant (blue) standing light wave at 811 nm. The absorptive grating was set up with a thin standing light wave (thickness <1 mm, 801 nm on resonance) directly behind the refractive crystal.

The experimentally observed behavior of the total wave field for the two conjugate Bragg incidences is shown in Fig. 14. In the upper graph the near field for a weak potential is measured continuously in a range between the two conjugate first Bragg orders. Due to dynamical diffraction theory the diffraction efficiencies in the two conjugated orders are given by exchanging G with $-G$. Thus from Eq. (18) it follows that the atomic wave field for conjugated incidence should be shifted by π as confirmed by the experimental data of Fig. 14.

In order to demonstrate the behavior more clearly, the lower graph of Fig. 14 shows a one-dimensional cut through the data of the upper graph, taken at Bragg incidence (‘‘ +Bragg’’). The dashed curve indicates the fraction of the light intensity of the absorptive grating, that is in phase (‘‘overlapping’’) with the intensity nodes of the first Bragg crystal. The steep rise of the intensity at the right side (corresponding to the black vertical stripe in the upper plot) is due to the shadow of the mirror edge. Since we know that at the mirror surface the light crystal is in phase with the absorptive mask, we can deduce the absolute position of the atomic wave field emerging from the Bragg crystal. The data show that the total wave field inside a blue detuned light crystal has its maxima at the steepest gradient of the potential on which the incident wave impinges. These results agree with the predictions of dynamical diffraction theory.

Furthermore, one can investigate the wave field as a function of the incidence angle, since the mask (thin optical element) does not depend critically on the incidence angle as discussed in Sec. II. Experimental results are shown in Fig. 15 in comparison with the predictions of dynamical diffraction theory. We measured for every incidence angle both the near field, using the masking technique described above, and the far field after switching off the thin standing light wave. This led to a measurement time of 10 hours for each set of data. The upper three graphs represent the measured Bragg and forward scattered intensities found by fitting the measured far field pattern for the three different potential heights. The solid lines represent the predictions of dynamical diffraction theory with only the potential height as a free fit parameter. The middle three graphs show the results of the corresponding near field measurements. The dark bar at the top of the middle graphs represents the mirror surface (minus 5 μm due to the gray scale mapping of the graph). This marker is missing on the middle right graph, because the start position of the motor drifted during the experiment, whereas the position measurement was still accurate. The zero position (mirror surface) was then calibrated after the measurement. The lower graphs show the predictions of dynamical diffraction theory without any new fitting parameter. It is important to note that the gray scale is the same for the three experimental graphs and for the three theoretical graphs. Thus in addition to the explanation of the shift of the wave field by dynamical diffraction theory even the contrast of the wave field modulation as a function of potential height is confirmed.

In order to get an agreement between theory and experi-

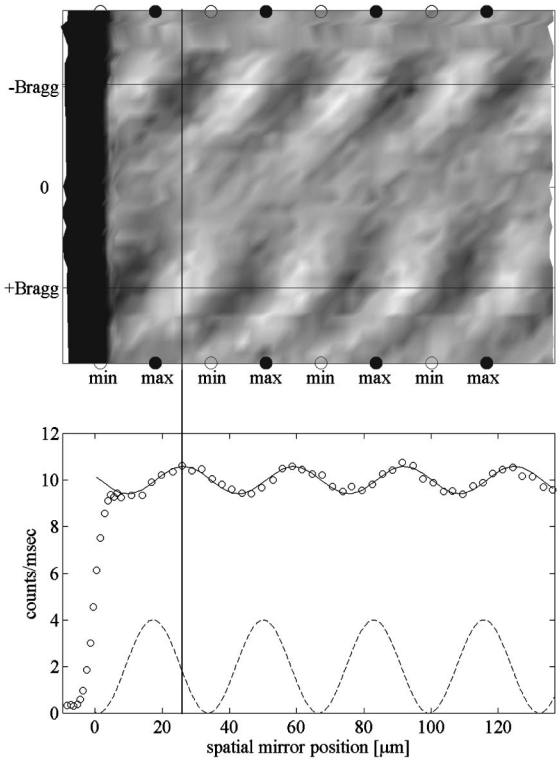

FIG. 14. Where do atoms incident at the Bragg angle leave a refractive crystal? The near field measurement for atomic incidence angles between the two conjugate Bragg orders (upper graph) shows that the wave fields for conjugate Bragg incidences leave the crystal at opposite flanks of the potential as predicted by dynamical diffraction theory. The circles represent the potential minima and maxima. The black bar on the left is the shadow of the mirror (distorted by the gray scale mapping). Furthermore, the data allow for determining the absolute position of the maximum of the atomic wave field: The lower plot shows a one-dimensional cut through the data of the upper graph, taken at Bragg incidence (the dashed curve indicates the beating phase between the two successive gratings—which are exactly in phase at the mirror surface). The data show that the atomic wave field emerging from a *refractive* Bragg crystal is shifted by $\pi/2$ with respect to the crystal planes, i.e., its distance to the closest node of the blue detuned standing light wave deduced from this measurement is (90 ± 15) nm, corresponding to a quarter of a grating period.

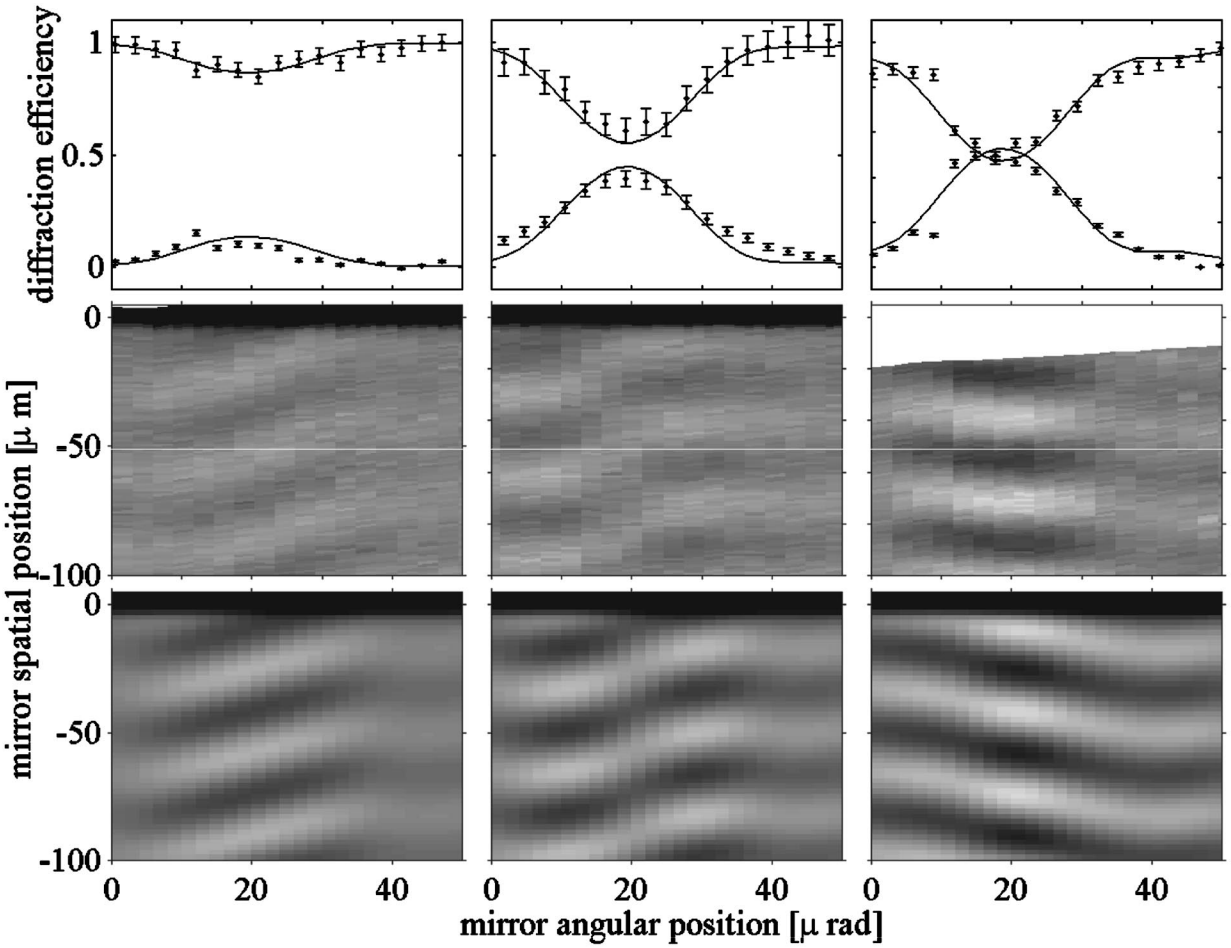

FIG. 15. Near and far field measurements behind a light crystal compared with dynamical diffraction theory. The upper graphs show the forward (upper trace) and Bragg scattered intensities (lower trace) as a function of the incidence angle. The solid lines are results of dynamical diffraction theory, where the potential height was assumed to be a free parameter. The middle graphs are measured near field patterns as a function of the incidence angle. Brighter regions in the density plots correspond to higher atomic intensities. The lower graphs represent the corresponding results of dynamical diffraction theory for the near field.

ment one has to take into account the velocity distribution, and more importantly the divergence of the incident beam. This divergence of ± 8 μrad was deduced from the width of the far field slit pattern which was for these measurements 27 μm (FWHM). This angular divergence mainly explains the reduced contrast of the wave field modulation for exact Bragg incidence in the case of an intermediate potential height. Deducing the expected near field interference pattern via the observed scattered intensities in the far field one would expect maximal contrast at Bragg incidence. The observed minimum of the atomic intensity modulation results from the incoherent superposition of the total wave fields corresponding to each incidence angle. However, this does not show up in the far field where the intensities for the different incidence angles are added up. Thus the near field measurement reveals information about the transverse coherence length of the incident beam.

Based on these results we will show in the following that in the case of absorptive light crystals only one of the basic Bloch states contributes to the diffracted intensity.

VII. PURE ABSORPTIVE CRYSTAL

The experiments of this section have been partially described in a previous publication [6]. However, the main results will be discussed again briefly in the vicinity of the other investigations, and with direct absolute comparison between dynamical diffraction theory and experimental results.

A standing light wave with a laser exactly tuned on resonance with the open transition at 801 nm represents a periodic imaginary potential as discussed in Sec. IV. The values of the relevant Fourier components of the potential are

$$V_0 = -i\frac{V_{\max}}{2},$$

$$V_G = -i\frac{V_{\max}}{4}e^{i\alpha}, \tag{20}$$

$$V_{-G} = -i\frac{V_{\max}}{4}e^{-i\alpha}.$$

In contrast to the phase crystal the dc Fourier amplitude is imaginary and hence describes the average absorption of the incident beam instead of refraction. Since the evolution inside such a potential is not unitary (probability not conserved) the first Fourier components do not form a pair of complex conjugates.

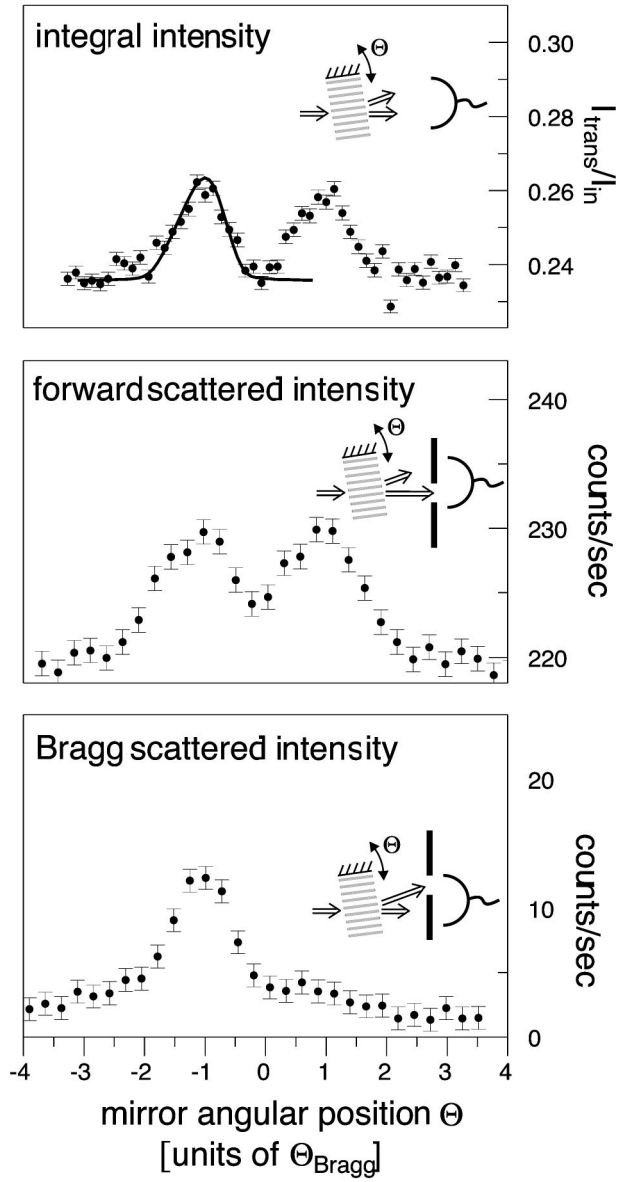

FIG. 16. Experimental rocking curves for a pure absorptive crystal: The upper graph shows the integral transmission through an absorptive light crystal as a function of the incidence angle. The increase of total transmission at Bragg incidence is known as the Borrmann effect. The solid line is a prediction of dynamical diffraction theory with no fitting parameters. The lower two graphs show that both the forward and the Bragg scattered intensities increase by the same amount, as predicted by dynamical diffraction theory.

A. Scattered intensity measurements

The diffraction of waves from an extended periodic absorptive structure is a situation where the decomposition of the total wave field into eigenfields is unveiled. In the case of periodic absorption the eigenfields experience different absorption due to their different spatial overlap with the absorptive structure. Thus, after a sufficiently long interaction distance mainly the minimal coupling state will survive. Consequently, the total wave field behind the crystal is determined by this minimal overlapping state, consisting of plane waves of equal amplitudes transmitted and diffracted. The total wave field has its maxima at the positions of minimal absorption, i.e., at the nodes of the standing light wave. For the experimental demonstration of this fact, we refer the reader to a previous publication [6], where the absolute phase of the atomic wave fields behind absorptive and refractive light crystals was measured with a method similar to that described in the preceding section (see Fig. 14). There it turned out that the atomic wave fields behind refractive and absorptive crystals are shifted by $\pi/2$ with respect to each other. Combining these results with the absolute measurements of the wave field position behind refractive crystals (preceding section) then actually demonstrates that the wave field behind an absorptive crystal emerges at the nodes of the potential.

This behavior has an interesting consequence, which appears when investigating the diffraction behavior as a function of the atomic incidence angle: These experimentally observed rocking curves for the pure absorptive crystal are shown in Fig. 16. The main difference compared to the experiments with the phase crystal is that the integral transmitted intensity exhibits maxima at the Bragg incidences. This is no violation of particle conservation since it is due to a reduced absorption. The increased transmission at Bragg incidence is known in x-ray diffraction as the Borrmann effect or *anomalous transmission*. It was observed by Borrmann for x rays in perfect crystals in 1941 [5]. Later this effect was demonstrated for electrons, neutrons [24], and in our group for atoms [6].

This behavior can be understood by considering the eigenfields. The off-Bragg absorption is then given by the spatial average of the absorptive structure, which is the dc Fourier component of the potential. The transmitted intensity is given by Beer's law in Eq. (14) as discussed in Sec. IV. For the on-Bragg situation one has to deal with two equally populated eigenfields which experience different absorption due to their different spatial overlap with the absorptive structure. Following Sec. III we get for the wave vector components $K_z^{\pm}$

$$K_z^- = \left\{1+\frac{i}{2}\left(\frac{V_{\max}}{2E}+\frac{V_{\max}}{4E}\right)\right\}k_z = k_z + i\frac{3}{4}\kappa,$$
$$K_z^+ = \left\{1+\frac{i}{2}\left(\frac{V_{\max}}{2E}-\frac{V_{\max}}{4E}\right)\right\}k_z = k_z + i\frac{1}{4}\kappa, \tag{21}$$

where κ is the mean absorption coefficient as introduced in Sec. IV. The scattered intensities are given as the coherent sum of the amplitudes of the eigenfields in the corresponding directions. For Bragg incidence one gets

$$I_G = \frac{1}{4}\left|e^{-(3/4)\kappa z}-e^{-(1/4)\kappa z}\right|^2 = \frac{1}{4}e^{-\kappa z}\left(e^{(\kappa/2)z}+e^{-(\kappa/2)z}-2\right),$$
$$I_0 = \frac{1}{4}\left|e^{-(3/4)\kappa z}+e^{-(1/4)\kappa z}\right|^2 = \frac{1}{4}e^{-\kappa z}\left(e^{(\kappa/2)z}+e^{-(\kappa/2)z}+2\right). \tag{22}$$

Calculating the total transmitted intensities for Bragg incidence and off-Bragg incidence, one finds for their difference

$$I_0 + I_G - I = 2I_G > 0. \tag{23}$$

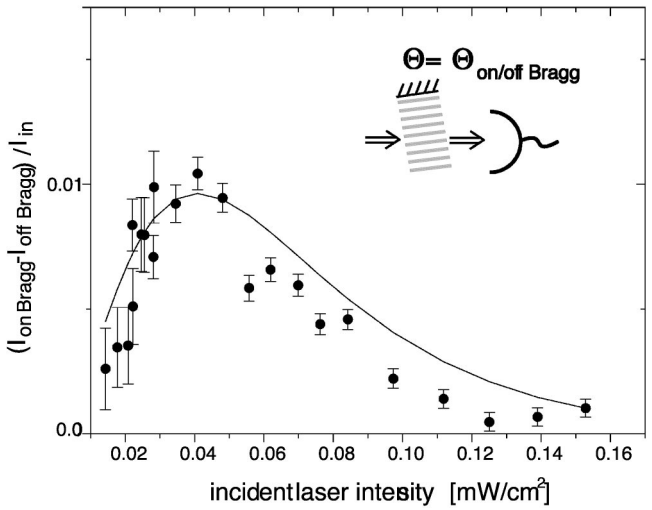

FIG. 17. Increase in the total transmission through an absorptive crystal at Bragg incidence as a function of the incident laser intensity. The solid curve indicates the theoretical behavior according to Eq. (24) (adapted for an incidence angle of θ_B+10 μrad). No Pendel behavior arises due to the fact that the accumulated phase difference of the eigenfields is imaginary.

Thus for Bragg incidence, the transmittance is always higher than expected from the average absorption.

Our experimental results shown in Fig. 16 for the integral, forward, and Bragg scattered intensities reveal the discussed features. The experimental results for the total transmission in Fig. 16 are compared with the theoretical prediction

$$I_G(z,V_G,\theta)=e^{-\kappa z}\frac{\sin^2\left[2\pi|V_G^s|z^s\sqrt{\frac{1}{4}(\theta_i^s/|V_G^s|)^2-1}\right]}{\frac{1}{4}(\theta_i^s/|V_G^s|)^2-1},$$

$$I_0(z,V_G,\theta)=e^{-\kappa z}+I_G(z,V_G,\theta). \tag{24}$$

These theoretical results reveal two main differences to the case of the phase crystal. The forward scattered intensity increases for Bragg incidence by the amount of the Bragg diffracted intensity as discussed above. Secondly no Pendel-like behavior is expected since the argument of the sine for reasonable values of θ^s and V_G^s is imaginary. A detailed theoretical discussion of the implication of a purely imaginary periodic potential in the Schrödinger equation is given by Berry and O'Dell [25].

B. Diffraction efficiency of absorptive crystals

The experimental results of the scattered intensity as a function of potential height are shown in Fig. 17. There we measured the ratio of the total throughput for on- and off-Bragg incidence as a function of laser light intensity. From the theory one expects that the maximal total increase of transmitted atoms is 7.2%. Taking into account velocity and angular distributions one would expect $\sim$2.7%. The fact that only a 1% transmission increase is observed might result from an angular misalignment of $\sim$10 μrad, which is on the order of our experimental accuracy for this experiment. Taking this misalignment into account one gets good agreement

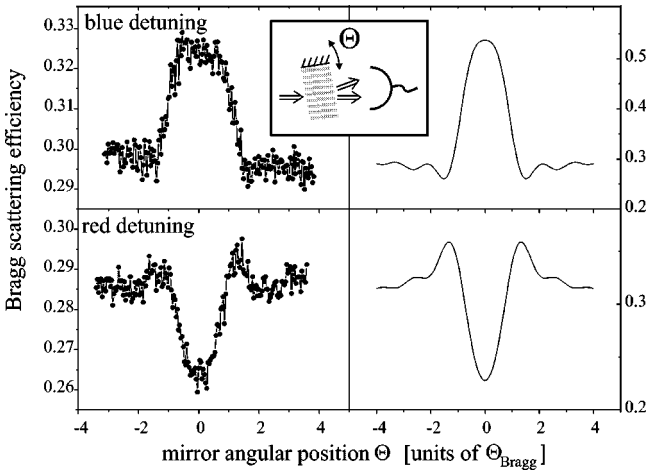

FIG. 18. The measured total transmission through a light crystal near resonance ($\pm$40 MHz): The left graphs show the total transmission for the indicated laser detunings. The right two graphs represent the results of dynamical diffraction theory. The qualitative behavior can be understood on the basis of the total wave field position determined by the real part of the potential and treating the absorption as a weak perturbation.

with theory. The data clearly demonstrate that no Pendellösung phenomenon arises, and that the maximum transmission is obtained at the expected potential height.

VIII. NATURAL LIGHT CRYSTAL

So far the description of a standing light wave as a pure phase or a pure absorptive crystal was only an approximation. For the far detuned case usually the residual absorption is neglected. The purity of the phase crystal can be defined as the ratio of imaginary to real parts of the potential, that is, $2\Delta/\Gamma$, where Γ is the linewidth and Δ is the detuning of the laser light from resonance. For our experiments with phase crystals the laser light was $\sim$5 GHz detuned from resonance leading to a phase/absorption purity of 1000. In the case of an exactly resonant light crystal the description as a pure absorptive structure neglects other possible transitions from the initial state. Since the laser is far detuned from those transitions they lead to an additional refractive contribution. Taking into account the nearest other transition in our experiment one finds an absorption/phase purity of 10^6.

In order to study the influence of the combination of imaginary and real potentials we measure the total transmission for a small detuning ($\pm$40 MHz). The experimental results are shown in Fig. 18. The dependence on the incidence angle can be understood on the basis of the total wave fields. The total wave field will be determined mainly by the refractive crystal, because the ratio of real to imaginary potentials is $\sim$20. Thus the absorption can be regarded as a small disturbance. The influence of the absorption can then be deduced from the individual overlap of the total wave field with the absorptive potential.

For incidence angles smaller than the Bragg angle mainly the minimal coupling wave field determines the evolution (see Fig. 2). This means that the overlap of the atomic wave field with the crystal potential is minimal. Thus this means for red detuned light crystals that the overlap of the atom with the light *intensity* is maximal, corresponding to maxi-

mal absorption, whereas the overlap is minimal in the case of a blue detuned crystal leading to a minimal absorption. For incidences larger than the Bragg angle the situation is reversed. This is due to the fact that mainly the maximal coupling state determines the evolution. Therefore a lower absorption is found for the red detuned crystal and a higher absorption for the blue detuned light crystal.

The right hand graphs in Fig. 18 represent the results of dynamical diffraction theory with a ratio of 20/1 of refractive to absorptive contributions. The total potential height was assumed to be a free parameter to get the best agreement with the experimental data. The underlying theory as discussed so far is a two-beam approximation and therefore describes only one scattered beam in addition to the transmitted beam at a time. The theoretical curves shown are the normalized sum of the results for Bragg and conjugated Bragg incidences calculated individually and added up incoherently. Thus we do not take into account interference effects between the plus and the minus Bragg diffracted amplitudes (note that this approach is most critical at exactly perpendicular incidence, where two beams diffracted at the two conjugated first diffraction orders should contribute with equal efficiencies, in addition to the transmitted beam). Nevertheless, a numerical integration of the Schrödinger equation (multiple-beam dynamical diffraction theory, including eight beams) leads to the same qualitative results for our weak scattering potentials, i.e., it yields qualitatively the same functional dependence of the total transmission on the incidence angle, and on the frequency detuning of the light potential. The experimental results should be understood as qualitative results for scattering from a complex potential. A more detailed discussion for complex light crystals is given in the following section.

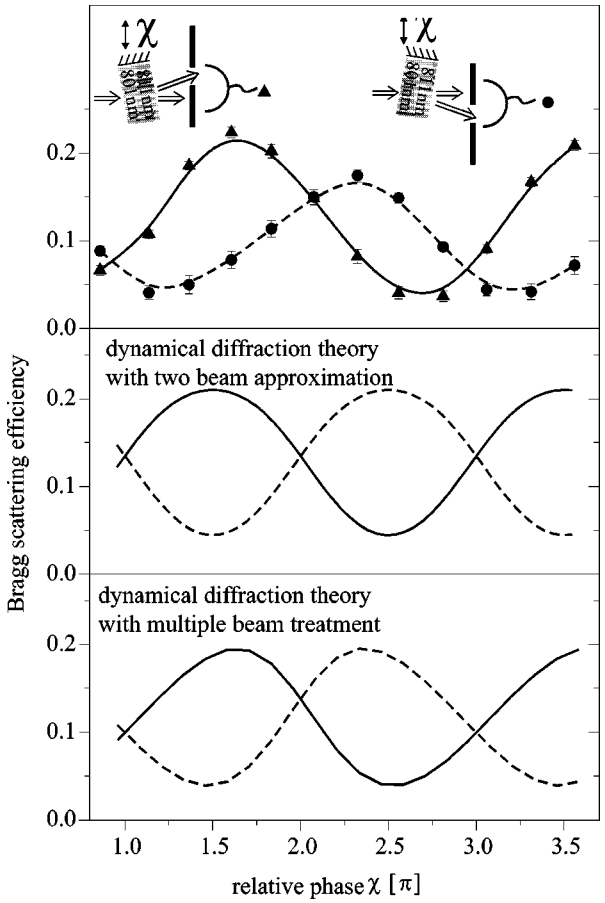

FIG. 19. Bragg scattered intensity for Bragg and conjugate Bragg incidence as a function of the relative phase between absorptive and refractive parts of the potential: The lower two graphs show the results of dynamical diffraction theory, within the two-beam approximation, and multiple-beam treatment, respectively. Clearly a violation of Friedel's law, stating that the diffraction efficiency is the same for both conjugate Bragg incidences, is observed.

IX. COMPLEX LIGHT CRYSTAL

So far we have not utilized the fact that light fields can be arbitrarily superposed and thus one can model the most general complex periodic potential for first order Bragg diffraction where only the first Fourier transform amplitudes of the potential are of relevance. The possibility to create such complex potentials has been demonstrated in a previous publication [8]. Superposing a pure absorptive crystal at 801 nm (resonant light) and a phase crystal at 811 nm (off-resonant light) allows for the realization of a potential of the general form

$$V(x)=V_r[1+\cos(Gx)]+iV_i[1+\cos(Gx+\chi)], \quad (25)$$

where V_i and V_r represent the amplitudes of the absorptive and refractive parts, respectively.

The Fourier amplitudes are then given by

$$V_0=V_r+iV_i,$$

$$V_G=\frac{V_r+iV_ie^{i\chi}}{2}, \quad (26)$$

$$V_{-G}=\frac{V_r+iV_ie^{-i\chi}}{2}.$$

Experimentally the relative spatial phase χ between real and imaginary part at the incidence position of the atomic beam is controlled by the mirror position as described in Sec. V.

The experimental results for the diffraction efficiencies for such a composed potential are shown in the upper plot of Fig. 19. In contrast to the previous results, the diffraction efficiencies for Bragg incidence and conjugate Bragg incidence are different for all relative phases with the exceptions of $\chi=0,\pi,2\pi,\ldots$. These phases correspond to the situation of a ''natural'' complex crystal discussed in Sec. VIII. For those cases the Fourier amplitudes are symmetric.

The mathematical description within the framework of dynamical diffraction theory is straightforward. The connection between the results for Bragg and conjugated Bragg incidence follows formally by replacing G with $-G$. This does not change the absolute value of the wave vectors inside the crystal [see Eq. (9), Sec. III] and thus the accumulated phase difference between the eigenfields is the same for both Bragg incidences. However, the amplitudes of the plane waves in the Bragg direction $A_{\pm}$ change [Eq. (10), Sec. III] and are connected by the relation

$$A_{\pm}^{-G}=\frac{V_{-G}}{V_G}A_{\pm}^{G}. \tag{27}$$

Using the general result for the Bragg scattered intensity [Eq. (12), Sec. III] the diffracted intensity for Bragg and conjugated Bragg incidence are given by

$$I_G=\frac{|V_G|^2}{V_{-G}V_G}|e^{iK_z^+L}+e^{iK_z^-L}|^2,$$
$$I_{-G}=\frac{|V_{-G}|^2}{V_{-G}V_G}|e^{iK_z^+L}+e^{iK_z^-L}|^2. \tag{28}$$

The prediction of this theory is shown in the middle graph of Fig. 19. The oscillatory behavior as a function of the relative phase χ results from the dependence of the diffracted intensity on the absolute square value of the corresponding Fourier component. The observed distortion of the sinusoidal behavior arises since the two-beam approximation does not hold for the high potentials experimentally used. For a more quantitative description one has to take into account higher diffraction orders (multiple-beam treatment). The numerical solution of the Schrödinger equation in an eight-beam approximation is shown in the lower graph of Fig. 19 and reproduces the observed asymmetry. It is noteworthy that the maximal absolute diffraction efficiencies are the same for both theoretical treatments.

The different behavior for Bragg and conjugated Bragg incidence can be regarded as a violation of Friedel's law [26]. This is an empirical law stated by Friedel in 1913, which claims that the diffraction behavior does not change if a periodic structure is inverted at any point. This implies that for a given crystal both Bragg and conjugated Bragg orders should have the same intensities. However, the results of the dynamical diffraction theory given in Eq. (28) show that Friedel's law is *only* fulfilled if the absolute values of the conjugate Fourier amplitudes of the potential are identical, since

$$I_G=I_{-G}\leftrightarrow|V_G|^2=|V_{-G}|^2. \tag{29}$$

Thus, Friedel's empirical law cannot be broken by any purely refractive, or purely absorptive crystal, even if the elementary cell has no inversion symmetry. However, for combined absorptive and refractive structures this rule is generally violated, except in the case of a ''natural'' crystal where real and imaginary crystals are exactly in or out of phase.

Since the general formulas are quite lengthy we discuss one extreme case of a complex potential, namely,

$$V=V_0+V_Ge^{iGx}. \tag{30}$$

This potential can be realized by superposing a refractive crystal and an absorptive crystal with a relative phase of $\pi/2$. For such a potential with $V_{-G}=0$ it turns out that the first term in Eq. (28) for the Bragg diffraction efficiency diverges. Nevertheless, a finite diffraction efficiency is found, since the second term approaches zero for the limit $V_{-G}\rightarrow 0$. The diffracted intensities are given by

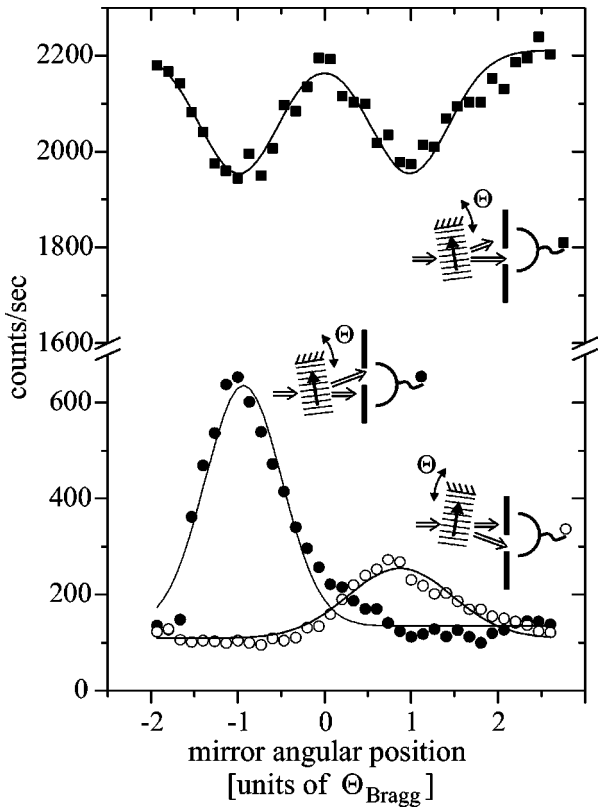

FIG. 20. The experimentally observed rocking curves for a potential of the special form $V(x)=1-i+e^{iGx}$: The forward scattered intensity is indicated with squares (upper curve) and Bragg scattered intensities are given by the two lower curves for the two conjugate Bragg orders indicated with open and solid circles, respectively. This special potential was realized by choosing a relative spatial phase of $\pi/2$ between two overlapping refractive and absorptive crystals. This case leads to an extreme violation of Friedel's law, i.e., a complete suppression of Bragg scattering at one of the two conjugate Bragg orders. The experimentally observed residual scattering is due to different values of the absorptive and the refractive part of the potential.

$$I_0=e^{-\kappa z},$$
$$I_G=(4\pi z^s V_r^s)^2e^{-\kappa z}, \tag{31}$$
$$I_{-G}=0,$$

where κ is the mean absorption coefficient as defined in Sec. IV. Thus the forward scattered intensity should exhibit no angular dependence. The diffracted intensity is given purely by an anomalously transmitted contribution. The corresponding experimental data are shown in Fig. 20.

Obviously the diffraction efficiency in the two conjugate first Bragg orders is extremely different, although the experimental geometries are symmetric (see inset in Fig. 20). Since the forward diffracted intensities (upper curve) are identical for both incidences, the increased diffraction efficiency at one of the Bragg angles is given *only* by anomalously transmitted atoms. The residual dependence of the forward scattered intensity on the incidence angle follows from the fact that the absorptive potential was only about half of the refractive potential. This also gives rise to a small diffraction efficiency in the conjugate Bragg order, which is supposed to

be completely suppressed in the ideal case. Diffraction experiments at such a complex potential and their relation to Friedel's law are discussed theoretically by Berry [27].

X. CONCLUSION

We have shown that atomic de Broglie waves can be a model system for diffraction experiments. By utilizing the interaction of light with the internal states of an atom one can model media for de Broglie waves of both refractive and absorptive characters with a huge variety of spatial configurations. Superpositions of standing light waves allow the realization of potentials which were not accessible previously. The big advantage of the atom-light system with respect to optical experiments is that the character of the diffracting structure is readily changeable because it is only determined by the detuning of the light frequency with respect to the atomic transition frequency. Additionally, the coupling strength between atoms and light is proportional to the light intensity. This makes new experiments feasible, e.g., investigation of the Pendellösung phenomenon as a function of crystal potential, which shows new features compared to the usually investigated dependence on the effective crystal length. We discussed our experimental results within the framework of the well known dynamical diffraction theory for pure refractive, pure absorptive, and for tailored complex potentials. The observed diffraction efficiencies and diffraction phases were well explained by this theory.

ACKNOWLEDGMENTS

This work was supported by the Austria Science Foundation (FWF) under Project No. S06504, and by the European Union as part of TMR Grant No. EBR-FMRX-CT96-0002.

[1] B. W. Batterman and H. Cole, Rev. Mod. Phys. **36**, 681 (1964).
[2] S. Adams, M. Sigel, and J. Mlynek, Phys. Rep. **240**, 143 (1994).
[3] V. I. Balykin and V. S. Letokhov, *Atom Optics with Laser Light* (Harwood Academic, Chur, Switzerland, 1995).
[4] For an overview on atomic interferometry see *Atom Interferometry*, edited by P. Berman (Academic Press, New York, 1997).
[5] G. Borrmann, Phys. Z. **42**, 157 (1941).
[6] M. K. Oberthaler, R. Abfalterer, S. Bernet, J. Schmiedmayer, and A. Zeilinger, Phys. Rev. Lett. **77**, 4980 (1996).
[7] R. Abfalterer, C. Keller, S. Bernet, M. K. Oberthaler, J. Schmiedmayer, and A. Zeilinger, Phys. Rev. A **56**, R4365 (1997).
[8] C. Keller, M. K. Oberthaler, R. Abfalterer, S. Bernet, J. Schmiedmayer, and A. Zeilinger, Phys. Rev. Lett. **79**, 3327 (1997).
[9] P. P. Ewald, Ann. Phys. (Leipzig) **54**, 519 (1917); this is elaborated further in W. H. Zachariasen, *Theory of X-ray Diffraction in Crystals*, 2nd ed. (Dover Publications, Inc., New York, 1994).
[10] H. Bethe, Ann. Phys. (Leipzig) **87**, 55 (1928); this is elaborated further in [14].
[11] M. L. Goldberger and F. Seitz, Phys. Rev. **71**, 294 (1947); elaborated in [17].
[12] H. F. Talbot, Philos. Mag. **9**, 401 (1836).
[13] H. J. Juretschke, D. W. J. Cruickshank, and N. Kato, *P. P. Ewald and his Dynamical Theory of X-ray Diffraction*, IUCr Monographs on Crystallography Vol. 2 (Oxford University Press Inc., New York, 1992); P. P. Ewald, Z. Kristallogr. **93**, 396 (1936).
[14] J. M. Cowley, *Diffraction Physics* (North-Holland, Amsterdam, 1990).
[15] C. Salomon, J. Dalibard, A. Aspect, H. Metcalf, and C. Cohen-Tannoudji, Phys. Rev. Lett. **59**, 1659 (1987).
[16] N. W. Ashcroft and N. D. Mermin, *Solid State Physics* (Holt-Saunders, New York, 1976).
[17] H. Rauch and D. Petrascheck, in *Neutron Diffraction*, edited by H. Dachs (Springer, New York, 1978), p. 303.
[18] D. O. Chudesnikov and V. P. Yakovlev, Laser Phys. **1**, 110 (1991).
[19] J. Kawanaka, K. Shimizu, and H. Takuma, Appl. Phys. B: Photophys. Laser Chem. **56**, 21 (1993).
[20] P. J. Martin, B. G. Oldaker, A. H. Miklich, and D. E. Pritchard, Phys. Rev. Lett. **60**, 515 (1988); S. Kunze, S. Dürr, G. Rempe, Europhys. Lett. **34**, 343 (1996); S. Dürr, S. Kunze, and G. Rempe, Quantum Semiclassic. Opt. **8**, 531 (1996); D. M. Giltner, R. W. McGowan, and S. A. Lee, Phys. Rev. A **52**, 3966 (1995).
[21] A. F. Bernhardt and B. W. Shore, Phys. Rev. A **23**, 1290 (1981).
[22] D. Sippel, K. Kleinstück, and G. E. R. Schulze, Phys. Lett. **14**, 174 (1965).
[23] C. G. Shull, Phys. Rev. Lett. **21**, 1585 (1968).
[24] For x rays: G. Borrmann, Z. Phys. **42**, 157 (1942); for neutrons: S. Sh. Shilshtein, V. J. Marichkin, M. Kalanov, V. A. Somenkov, and L. A. Sysoev, Zh. Éksp. Teor. Fiz., Pis'ma Red. **12**, 80 (1970) [JETP Lett. **12**, 56 (1970)]; A. Mazel and R. Ayroles, J. Microsc. **7**, 793 (1968).
[25] M. V. Berry and D. H. J. O'Dell, J. Phys. A **31**, 2093 (1998).
[26] M. G. Friedel, C.R. Hebd. Seances Acad. Sci. **157**, 1533 (1913).
[27] M. V. Berry, J. Phys. A **31**, 3493 (1998).